TWMS J. App. and Eng. Math. V.13, N.1, 2023, pp. 152-165

APPLYING MULTIQUADRIC QUASI-INTERPOLATION TO SOLVE FOKKER-PLANCK EQUATION

M. RAHIMI[1], H. ADIBI[1*], M. AMIRFAKHRIAN[1,2], §

Abstract. The Fokker-Planck equation (FPE) arises in various fields in physics, chemistry, natural science. It is difficult to obtain analytical solutions, accordingly we resort to numerical methods. In this study, we present a meshfree method to solve FPE. It is based on the multiquadric quasi-interpolation (MQQI) operator $\mathcal{L}_{W_2}$ and collocation technique. Here, θ-weighted finite difference scheme is used to discretize the temporal derivative. Then, the unknown function and its spatial derivatives are approximated by the multiquadric quasi-interpolation (MQQI) operator $\mathcal{L}_{W_2}$. Furthermore, the stability of the technique is investigated. This method is applied to some examples and the numerical results have been compared with the exact solutions and results of another method.

Keywords: Fokker-Planck equation, multiquadric quasi-interpolation, θ-weighted finite difference method, collocation method, meshless method.

AMS Subject Classification: 35Q84, 65M06.

1. Introduction

The Fokker-Planck equation (FPE) is a partial differential equation is derived from the Stochastic Differential Equation (SDE) With the help of Itô calculus. FPE is used in a wide variety of physics, biology and chemistry such as solid-state physics, circuit theory and theoretical biology [9, 22].

This differential equation is mainly applicable in probability density. For some application of this equation, we refer the interested reader to [15, 16, 32].

Fokker and Planck utilized the FPE to investigate the Browninan motion of particles [22]. The general representation of the FPE for the variable x is given [5, 22, 24]:

$$\frac{\partial u}{\partial t} = \left[-\frac{\partial}{\partial x}A(x) + \frac{\partial^2}{\partial x^2}B(x)\right] u, \ (x \in [a,b],\, t \geqslant 0), \tag{1}$$

[1] Department of Mathematics, Central Tehran Branch, Islamic Azad University, Tehran, Iran.
e-mail: rahimi_mah@yahoo.com; ORCID: https://orcid.org/0000-0002-1315-4901.
e-mail: adibih@aut.ac.ir; ORCID: https://orcid.org/0000-0002-8167-5020.
* Corresponding author.
e-mail: amirfakhrian@iauctb.ac.ir; ORCID: https://orcid.org/0000-0001-9934-6412.
[2] Department of Computer Science, University of Calgary, Canada.
e-mail: majid.amirfakhrian@ucalgary.ca.
§ Manuscript received: October 16, 2020; accepted: January 07, 2021.
TWMS Journal of Applied and Engineering Mathematics, Vol.13, No.1

with initial and boundary conditions:

$$u(x,0) = f(x),\ u(a,t) = g_a(t),\ u(b,t) = g_b(t) \tag{2}$$

where $f(x)$, $g_a(t)$ and $g_b(t)$ are all known functions. In Eq. (1), $B(x) > 0$ is called the diffusion coefficient and $A(x)$ is the drift coefficient. These coefficients could be in terms of x and t, i.e.:

$$\frac{\partial u}{\partial t} = \Big[-\frac{\partial}{\partial x}A(x,t) + \frac{\partial^2}{\partial x^2}B(x,t)\Big]u. \tag{3}$$

The Eq. (3) describes the motion of the concentration field u, which is a linear parabolic partial differential equation. This is exactly a diffusion equation which also involves first order derivative with respect to x. This equation is also known as forward Kolmogorov equation.

It is notable that the backward Kolmogorov equation is as follows [22, 24]:

$$\frac{\partial u}{\partial t} = -\Big[A(x,t)\frac{\partial}{\partial x} + B(x,t)\frac{\partial^2}{\partial x^2}\Big]u. \tag{4}$$

The most general form of Eq. (1) appears as:

$$\frac{\partial u}{\partial t} = \Big[-\sum_{i=1}^{J}\frac{\partial}{\partial x_i}A_i(x) + \sum_{j,i=1}^{J}\frac{\partial^2}{\partial x_i \partial x_j}B_{i,j}(x)\Big]u, \tag{5}$$

$$u(x,0) = f(x), \quad \big(x = (x_1, x_2, \ldots, x_J) \in \mathbb{R}^J\big), \tag{6}$$

which involves J variables. Note that the non-linear form of the FPE, is as follows:

$$\frac{\partial u}{\partial t} = \Big[-\frac{\partial}{\partial x}A(x,t,u) + \frac{\partial^2}{\partial x^2}B(x,t,u)\Big]u. \tag{7}$$

This equation has significant applications in biophysics, plasma, surface physics, neuroscience, nonlinear hydrodynamics, marketing and psychology [22, 24]. Various numerical methods for solving FPEs have been proposed. In [18] a fast algorithm with high accuracy has been proposed. Reif and Barakat [21] used Chebyshev technique for solving 1-D time independent FPE. However, the numerical methods for solving FPEs are mainly Finite difference method (FDM) for 2D-case [33], Variational iteration method (VIM) [7], moving Finite element method (FEM) [11], Homotopy perturbation method (HPM) [13] and Adomian decomposition method [24]. The Radial basis function (RBF) method was first studied by Hardy [10], which reveals excellent interpolant, especifically for scattered data in high dimensions. Various applications of RBF method have been extensively investigated in [6, 8, 28, 29]. Also, RBF techniques have been studied by Ballestra and Pacelli [3].

Unfortunately, these meshless methods require solving an ill-conditioned linear system [1, 27]. So modified meshless schemes have been developed.

Beaston and Powell proposed three types of univariate MQQIs known as $\mathcal{L}_A, \mathcal{L}_B$ and $\mathcal{L}_C$ [4]. Wu and Schaback [30], presented the MQQI operator $\mathcal{L}_D$. Jiang et al. [14] have recently presented a new multi-level univariate MQQI method based upon inverse multiquadric (IMQ) radial basis functions and $\mathcal{L}_D$ operator, namely as $\mathcal{L}_W$ and $\mathcal{L}_{W_2}$. Also, researchers in [12, 19, 31] proposed meshless technique for solving PDEs by employing MQQI, without needing to solve large linear systems.

In this paper we present a numerical meshless method based on MQQI operaor $\mathcal{L}_{W_2}$ to approximate the solution of the FPE by using collocation method and employ the θ-weighted finite difference method to estimate the temporal derivative.

The layout of this paper is as follows. In Section 2, we describe the MQ quasi-interpolation scheme. In Section 3, the method is applied on the Fokker–Planck equation. The stability analysis of the method is investigated in Section 4. In Section 5, numerical examples are tested to verify the effect of the proposed method. Finally, a brief conclusion is presented in Section 6.

2. The MQQI scheme

Considering the partition:

$$a = x_0 < x_1 < \cdots < x_n = b, \quad h = \max_{1 \leqslant i \leqslant n} (x_i - x_{i-1}), \tag{8}$$

on $\Omega = [a, b]$, the univariate real funtion f usually takes the following quasi-interpolation form:

$$\mathcal{L}(f) = \sum_{i=0}^{n} f(x_i)\Psi_i(x), \qquad (x_i \in [a, b]), \tag{9}$$

where each function $\Psi_i(x)$ is a multi-quadric radial basis funtion [10], defined by:

$$\Psi_i(x) = \left(c^2 + (x - x_i)^2\right)^{\frac{1}{2}}, \tag{10}$$

and $c > 0$ is a shape parameter. The MQQI operator $\mathcal{L}_D$ is introduced by Wu and Schaback as [30].

$$\mathcal{L}_D[f(x)] = \sum_{i=0}^{n} f(x_i)\tilde{\Phi}_i(x), \tag{11}$$

where

$$\begin{aligned}
\tilde{\Phi}_0(x) &= \frac{1}{2}\Big[1 + \frac{\Psi_1(x) - (x - x_0)}{(x_1 - x_0)}\Big], \\
\tilde{\Phi}_1(x) &= \frac{1}{2}\Big[\frac{\Psi_2(x) - \Psi_1(x)}{(x_2 - x_1)} - \frac{\Psi_1(x) - (x - x_0)}{(x_1 - x_0)}\Big], \\
\tilde{\Phi}_i(x) &= \frac{1}{2}\Big[\frac{\Psi_{i+1}(x) - \Psi_i(x)}{(x_{i+1} - x_i)} - \frac{\Psi_i(x) - \Psi_{i-1}(x)}{(x_i - x_{i-1})}\Big], \quad (2 \leqslant i \leqslant n-2), \\
\tilde{\Phi}_{n-1}(x) &= \frac{1}{2}\Big[\frac{(x_n - x) - \Psi_{n-1}(x)}{(x_n - x_{n-1})} - \frac{\Psi_{n-1}(x) - \Psi_{n-2}(x)}{(x_{n-1} - x_{n-2})}\Big], \\
\tilde{\Phi}_n(x) &= \frac{1}{2}\Big[1 + \frac{\Psi_{n-1}(x) - (x_n - x)}{(x_n - x_{n-1})}\Big].
\end{aligned} \tag{12}$$

Now, we choose a smaller set $\{x_{k_i}\}_{i=1}^{N}$ from the given points $\{x_i\}_{i=0}^{n}$, where N is a positive integer satisfying $N < n$ and $0 = k_0 < k_1 < \ldots < k_{N+1} = n$. Utilizing IMQ-RBF, the RBF interpolation of $S_{f''}$ can be represented by:

$$S_{f''}(x) = \sum_{j=1}^{N} \lambda_j \tilde{\varphi}_j(x), \tag{13}$$

where

$$\tilde{\varphi}_j(x) = \frac{p^2}{\left(p^2 + (x - x_{k_j})^2\right)^{\frac{3}{2}}}, \tag{14}$$

with the shape parameter $p \in \mathbb{R}^+$. The coefficients $\{\lambda_j\}_{j=1}^N$ are uniquely determined by the interpolation condition.

$$S_{f''}(x_{k_i}) = \sum_{j=1}^{N} \lambda_j \tilde{\varphi}_j(x_{k_i}) = f''(x_{k_i}), \quad (1 \leqslant i \leqslant N). \tag{15}$$

Due to the solvability of (15), [17], we get:

$$\lambda = A_X^{-1} \cdot F_X'', \tag{16}$$

where $X = \{x_{k_1}, x_{k_2}, \ldots, x_{k_N}\}$, $\lambda = \{\lambda_1, \lambda_2, \ldots, \lambda_N\}^T$, $A_X = \big[\tilde{\varphi}_j(x_{k_i})\big]$ and $F_X'' = \big[f''(x_{k_1}), f''(x_{k_2}), \ldots, f''(x_{k_N})\big]^T$.
Now, by using relation (16), an error function $e(x)$ is introduced by:

$$e(x) = f(x) - \sum_{i=1}^{N} \lambda_i \sqrt{p^2 + (x - x_{k_i})^2}. \tag{17}$$

If so, the operator $\mathcal{L}_{W_2}$ by utilizing $\mathcal{L}_D$ operator in relation (11) and (12) on $\{\big(x_i, e(x_i)\big)\}_{i=0}^n$ is defined by [23],

$$\mathcal{L}_{W_2} f(x) = \sum_{j=1}^{N} \lambda_j \sqrt{p^2 + (x - x_{k_j})^2} + \mathcal{L}_D e(x), \tag{18}$$

in which the constants c and p as shape parameters are not the same as in relation (18). Now, in relation (15), $f''(x_{k_i})$ can be replaced by [20]

$$f''(x_{k_i}) = \frac{\delta_x^2}{h_2^2(1 + 12\delta_x^2)} f(x_{k_i}), \tag{19}$$

with $h_2 = \frac{b-a}{N}$, where $\delta_x^2 f(x_{k_i}) = f(x_{k_{i+1}}) - 2f(x_{k_i}) + f(x_{k_{i-1}})$.

Which yields:

$$\sum_{j=1}^{N} \lambda_j \tilde{\varphi}_j(x_{k_i}) = \frac{\delta_x^2}{h_2^2(1 + 12\delta_x^2)} f(x_{k_i}), \quad (1 \leqslant i \leqslant N). \tag{20}$$

As a result, the coefficients $\{\lambda_j\}_{j=1}^N$ are determined uniquely via the linear system:

$$\lambda = A_X^{*-1} \cdot F_X'', \tag{21}$$

where $A_X^* = \big[(1 + 12\delta_x^2)\tilde{\varphi}_j(x_{k_i})\big]$. The accuracy and properties of $\mathcal{L}_W$ and $\mathcal{L}_{W_2}$, have been discussed in [14]. Now, we use MQQI operator $\mathcal{L}_{W_2}$ and equally spaced points. The compact form of operator $\mathcal{L}_{W_2}$ can be represented as [23]:

$$\mathcal{L}_{W_2} f(x) = \sum_{i=0}^{n} f(x_i) \hat{\Psi}_i(x). \tag{22}$$

3. The numerical method

Now, we use MQQI operator $\mathcal{L}_{W_2}$ to solve (1) numerically. Here, θ-weighted method along with collocation scheme are employed for approximating the temporal derivative. Consider the equation

$$\frac{\partial u}{\partial t} = \Big[- \frac{\partial}{\partial x} A(x,t) + \frac{\partial^2}{\partial x^2} B(x,t) \Big] u, \ (x \in [a,b], \ t \geqslant 0), \tag{23}$$

with initial and boundary conditions:

$$u(x,0)=f(x),\ u(a,t)=g_a(t),\ u(b,t)=g_b(t). \tag{24}$$

To solve (23), we descretize the problem by virtue of the following θ-weighted scheme,

$$\frac{u^{m+1}-u^m}{\Delta t}+\theta\Big[\frac{\partial}{\partial x}(Au)-\frac{\partial^2}{\partial x^2}(Bu)\Big]^{m+1}+(1-\theta)\Big[\frac{\partial}{\partial x}(Au)-\frac{\partial^2}{\partial x^2}(Bu)\Big]^{m}=0, \tag{25}$$

where $u^m=u(x,t_m)$, $t_m=m\Delta t$ and $\theta\in[0,1]$.

After some algebraic manipulations, the following time discretized form of linear FPE yields:

$$\begin{aligned}&u^{m+1}+\theta\Delta t\Big[\frac{\partial A^m}{\partial x}u^{m+1}+\frac{\partial u^{m+1}}{\partial x}A^m-\frac{\partial^2 B^m}{\partial x^2}u^{m+1}-2\frac{\partial B^m}{\partial x}\frac{\partial u^{m+1}}{\partial x}-B^m\frac{\partial^2 u^{m+1}}{\partial x^2}\Big]\\&=u^m+(\theta-1)\Delta t\Big[\frac{\partial A^m}{\partial x}u^m+\frac{\partial u^m}{\partial x}A^m-\frac{\partial^2 B^m}{\partial x^2}u^m-2\frac{\partial B^m}{\partial x}\frac{\partial u^m}{\partial x}-B^m\frac{\partial^2 u^m}{\partial x^2}\Big],\end{aligned} \tag{26}$$

where $A^m=A(x,t_m)$ and $B^m=B(x,t_m)$.

Now, we choose the nodes x_i, $i=0,1,2,\dots,n$ that x_i, $i=1,2,\dots,n-1$ are interior and x_0, x_n are boundary points in $[a,b]$ and approximate u^{m+1} using (22), by:

$$\begin{aligned}&u^{m+1}(x)=u(x,t_{m+1})\simeq\sum_{j=0}^{n}u_j^{m+1}\hat{\Psi}_j(x),\ u_x^{m+1}(x)=u_x(x,t_{m+1})\simeq\sum_{j=0}^{n}u_j^{m+1}\check{\Psi}_j(x),\\&u_{xx}^{m+1}(x)=u_{xx}(x,t_{m+1})\simeq\sum_{j=0}^{n}u_j^{m+1}\overline{\Psi}_j(x).\end{aligned} \tag{27}$$

By substituting (27) into (26) and (24), and applying collocations we deduce:

$$\begin{aligned}&\sum_{j=0}^{n}u_j^{m+1}\hat{\Psi}_j(x_i)+\theta\Delta t\Big[\frac{\partial A^m}{\partial x}(x_i)\sum_{j=0}^{n}u_j^{m+1}\hat{\Psi}_j(x_i)+A^m(x_i)\sum_{j=0}^{n}u_j^{m+1}\check{\Psi}_j(x_i)\\&-\frac{\partial^2 B^m}{\partial x^2}(x_i)\sum_{j=0}^{n}u_j^{m+1}\hat{\Psi}_j(x_i)-2\frac{\partial B^m}{\partial x}(x_i)\sum_{j=0}^{n}u_j^{m}\check{\Psi}_j(x_i)-B^m(x_i)\sum_{j=0}^{n}u_j^{m+1}\overline{\Psi}_j(x_i)\Big]\\&=u^m(x_i)+(\theta-1)\Delta t\Big[\frac{\partial A^m}{\partial x}(x_i)u^m(x_i)+\frac{\partial u^m}{\partial x}(x_i)A^m(x_i)-\frac{\partial^2 B^m}{\partial x^2}(x_i)u^m(x_i)\\&-2\frac{\partial B^m}{\partial x}(x_i)\frac{\partial u^m}{\partial x}(x_i)-B^m(x_i)\frac{\partial^2 u}{\partial x^2}(x_i)\Big].\end{aligned} \tag{28}$$

Also, by using boundary conditions and boundary nodes x_0, x_n, we have:

$$\sum_{j=0}^{n}u_j^{m+1}\hat{\Psi}_j(x_0)=g_a(t^{m+1}), \tag{29}$$

$$\sum_{j=0}^{n}u_j^{m+1}\hat{\Psi}_j(x_n)=g_b(t^{m+1}). \tag{30}$$

Eqs. (28), (29) and (30) form a system of $n+1$ linear equations with $n+1$ unknown u_i^{m+1}. These equations can be represented in matrix form and symbol $*$ stands for component

by component multiplication:

$$A_dU^{m+1}+\theta\Delta t\Big[A_2^m*(A_dU^{m+1})+A_1^m*(EU^{m+1})-B_3^m*(A_dU^{m+1})-2B_2^m*(EU^{m+1})$$
$$-B_1^m*(FU^{m+1})\Big]+A_bU^{m+1}=U^m+(\theta-1)\Delta t\Big[A_2^mU^m+A_1^mU_1^m-B_3^mU^m$$
$$-2B_2^mU_1^m-B_1^mU_2^m\Big]+G^{m+1}, \tag{31}$$

wherein

$$A_2^m=\Big[0,\frac{\partial A^m}{\partial x}(x_1),\dots,\frac{\partial A^m}{\partial x}(x_{n-1}),0\Big]^T,\ A_1^m=\Big[0,A^m(x_1),\dots,A^m(x_{n-1}),0\Big]^T,$$
$$B_3^m=\Big[0,\frac{\partial^2 B^m}{\partial x^2}(x_1),\dots,\frac{\partial^2 B^m}{\partial x^2}(x_{n-1}),0\Big]^T,\ B_2^m=\Big[0,\frac{\partial B^m}{\partial x}(x_1),\dots,\frac{\partial B^m}{\partial x}(x_{n-1}),0\Big],$$
$$B_1^m=\Big[0,B^m(x_1),\dots,B^m(x_{n-1}),0\Big]^T,$$

$$A_b=\begin{bmatrix}\hat\psi_{00}&\hat\psi_{10}&\cdots&\hat\psi_{n0}\\0&0&\cdots&0\\\vdots&\vdots&\ddots&\vdots\\0&0&\cdots&0\\\hat\psi_{0n}&\hat\psi_{1n}&\cdots&\hat\psi_{nn}\end{bmatrix},\ A_d=\begin{bmatrix}0&0&\cdots&0\\\hat\psi_{01}&\hat\psi_{11}&\cdots&\hat\psi_{n1}\\\vdots&\vdots&\ddots&\vdots\\\hat\psi_{0(n-1)}&\hat\psi_{1(n-1)}&\cdots&\hat\psi_{n(n-1)}\\0&0&\cdots&0\end{bmatrix},$$

$$E=\begin{bmatrix}0&0&\cdots&0\\\check\psi_{01}&\check\psi_{11}&\cdots&\check\psi_{n1}\\\vdots&\vdots&\ddots&\vdots\\\check\psi_{0(n-1)}&\check\psi_{1(n-1)}&\cdots&\check\psi_{n(n-1)}\\0&0&\cdots&0\end{bmatrix},\ F=\begin{bmatrix}0&0&\cdots&0\\\overline{\psi}_{01}&\overline{\psi}_{11}&\cdots&\overline{\psi}_{n1}\\\vdots&\vdots&\ddots&\vdots\\\overline{\psi}_{0(n-1)}&\overline{\psi}_{1(n-1)}&\cdots&\overline{\psi}_{n(n-1)}\\0&0&\cdots&0\end{bmatrix},$$

$$U^{m+1}=\begin{bmatrix}u_0^{m+1}\\u_1^{m+1}\\\vdots\\u_n^{m+1}\end{bmatrix},U_1^m=\Big[\frac{\partial u^m}{\partial x}(x_0),\dots,\frac{\partial u^m}{\partial x}(x_n)\Big]^T,U_2^m=\Big[\frac{\partial^2 u^m}{\partial x^2}(x_0),\dots,\frac{\partial^2 u^m}{\partial x^2}(x_n)\Big]^T.$$

$$\Big[A_d+A_b+\theta\Delta t\Big(A_2^m*A_d+A_1^m*E-B_3^m*A_d-2B_2^m*E-B_1^m*F\Big)\Big]U^{m+1}$$
$$=\Big[I+(\theta-1)\Delta t\big(A_2^m-B_3^m\big)\Big]U^m+(\theta-1)\Delta t\Big(A_1^mU_1^m-2B_2^mU_1^m-B_1^mU_2^m\Big)+G^{m+1}, \tag{32}$$

wherein

$$\begin{aligned}&M=A_2^m*A_d+A_1^m*E-B_3^m*A_d-2B_2^m*E-B_1^m*F,\\&\tilde A=A_b+A_d,\quad Q=\tilde A+\theta\Delta tM,\quad \tilde R=A_2^m-B_3^m,\\&K=(\theta-1)\Delta t(A_1^mU_1^m-2B_2^mU_1^m-B_1^mU_2^m)+G^{m+1},\\&R=I+(\theta-1)\Delta t\tilde R,\quad QU^{m+1}=RU^m+K,\end{aligned} \tag{33}$$

and

$$U^{m+1}=Q^{-1}RU^m+Q^{-1}K, \tag{34}$$

from (27) we have,

$$U^m = \tilde{A}U^m,$$

so

$$U^{m+1} = Q^{-1}R\tilde{A}^{-1}U^m + Q^{-1}K, \tag{35}$$

$$U^{m+1} = \tilde{A}Q^{-1}R\tilde{A}^{-1}U^m + \tilde{A}Q^{-1}K. \tag{36}$$

Despite, the validity of the method for any $\theta \in [0,1]$, we take $\theta = \frac{1}{2}$, as considered in Crank-Nicholson scheme.

4. Stability analysis

In order to show the stability, we obtain the amplification matrix first [25, 26]. Let U and $\tilde{U}$ be the difference and numerical solutions, respectively and $\varepsilon^{m+1} = U^{m+1} - \tilde{U}^{m+1}$ the error vector of Eq. (1), which can be written as

$$\varepsilon^{m+1} = \tilde{A}Q^{-1}R\tilde{A}^{-1}\varepsilon^m, \tag{37}$$

$$Q\tilde{A}^{-1}\varepsilon^{m+1} = R\tilde{A}^{-1}\varepsilon^m, \tag{38}$$

$$(I + \theta\Delta t M\tilde{A}^{-1})\varepsilon^{m+1} = (\tilde{A}^{-1} + (\theta-1)\Delta t\tilde{R}\tilde{A}^{-1})\varepsilon^m, \tag{39}$$

and

$$T = M\tilde{A}^{-1}, \qquad S = \tilde{R}\tilde{A}^{-1},$$

so, we have:

$$(I + \theta\Delta tT)\varepsilon^{m+1} = (\tilde{A}^{-1} + (\theta-1)\Delta tS)\varepsilon^m, \tag{40}$$

then

$$\varepsilon^{m+1} = (I + \theta\Delta tT)^{-1}(\tilde{A}^{-1} + (\theta-1)\Delta tS)\varepsilon^m, \tag{41}$$

where

$$\tilde{E} = (I + \theta\Delta tT)^{-1}(\tilde{A}^{-1} + (\theta-1)\Delta tS). \tag{42}$$

For stability issue, it is necessary that $\varepsilon^m \to 0$ as $m \to \infty$, i.e. $\rho(\tilde{E}) \leqslant 1$, where $\rho(\tilde{E})$ stands for spectral radius.

The stability condition is satisfied if

$$\left|\frac{\eta_{\tilde{A}^{-1}} + (\theta-1)\Delta t\eta_S}{1 + \theta\Delta t\eta_T}\right| \leqslant 1, \tag{43}$$

if $\theta = \frac{1}{2}$ we have:

$$\left|\frac{\eta_{\tilde{A}^{-1}} - \frac{\Delta t}{2}\eta_S}{1 + \frac{\Delta t}{2}\eta_T}\right| \leqslant 1, \tag{44}$$

where $\eta_{\tilde{A}^{-1}}$, η_S and η_T are the eigenvalues of the matrices $\tilde{A}^{-1}$, S and T, respectively.

5. Numerical examples

In this section, we present some numerical examples to show the robustness and accuracy of the presented method. The obtained results are compared to analytical results as well as the results in [2]. The L_2 and L_∞ error norms which are defined by:

$$L_2 = \|u^m - \tilde{u}^m\|_2 = \Big(\Delta x \sum_{j=0}^{n} |u^m(x_j) - \tilde{u}^m(x_j)|^2\Big)^{\frac{1}{2}},$$
$$L_\infty = \|u^m - \tilde{u}^m\|_\infty = \max_{0\leqslant j\leqslant n} |u^m(x_j) - \tilde{u}^m(x_j)|,$$

are used to measure the accuracy of our scheme where $u^m(x_j)$ and $\tilde{u}^m(x_j)$ represent the analytical and obtained numerical solutions, respectively at node j. For the sake of simplification, we set:

$$x_j = a + \frac{j(b-a)}{n}, \qquad j = 0, 1, \ldots, n.$$

In all examples we use $a = 0$, $b = 1$, $c = 10^{-9}$, $p = 2c$, $n = 10$, $n = 2N$, $\Delta t = 0.1$, $\Delta x = 0.1$, $\theta = \frac{1}{2}$.

The computations have been performed in Maple 17 on a PC with a CPU of 2.2 GHz.

Example 5.1. *Consider the FPE* (1) *with* $A(x) = -1$, $B(x) = 1$ *and* $u(x, 0) = x$, *which has the exact solution* $u(x, t) = x + t$. *The* L_∞ *and* L_2 *errors are listed in Table 1, at different times and our obtained results are compared with* [2]. *It is observed from Table 1 that the proposed method has better accuracy than* [2]. *Moreover, we use* $\Delta t = 0.1$ *but in* [2], $\Delta t = 0.01$ *was used. The spatial rate of convergence with* $\Delta t = 0.1$ *and different values of* n *for* $t = 0.3$ *are presented in Table 2. It can be seen from Table 2 that the convergence rate increases with the smaller spatial step size and the error norms increase slightly by increasing* n. *The graphs of top view of maximum error and absolute error over the space time with a color bar are shown in Figure 1. We also plot the graphs of absolute error and the estimated and analytical function at* $t = 1, 4, 10$ *in Figure 2.*

Table 1. The comparisons of the L_∞, L_2 errors of the presented method with the results of [2] at different times of Example 5.1.

t	*MQQI*		*method of* [2]	
	L_∞	L_2	L_∞	L_2
1	*1.90e-18*	*8.538e-19*	*1.900e-12*	*1.444e-12*
2	*3.00e-18*	*1.370e-18*	*2.900e-12*	*2.384e-12*
3	*4.10e-18*	*2.058e-18*	*3.900e-12*	*3.329e-12*
5	*6.40e-18*	*3.287e-18*	*5.899e-12*	*5.224e-12*
7	*8.60e-18*	*4.150e-18*	*7.899e-12*	*7.119e-12*
10	*1.19e-17*	*5.870e-18*	*1.090e-12*	*9.964e-12*

Table 2. The spatial rate of convergence at $t = 0.3$ with $\Delta t = 0.1$ of Example 5.1

n	L_∞	*Order*	L_2	*Order*
10	*1.12e-18*	—	*5.35e-19*	—
20	*2.5e-18*	*1.15*	*1.44e-18*	*1.43*
30	*2.38e-17*	*5.55*	*1.57e-17*	*5.90*
40	*5.43e-18*	*5.13*	*2.55e-18*	*6.33*
50	*3.11e-17*	*7.83*	*2.41e-17*	*10.07*

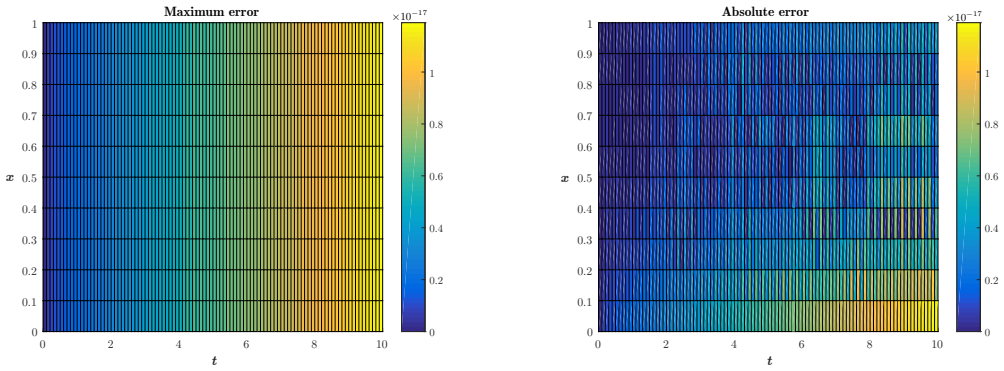

(a) (b)

FIGURE 1. Top view of the 3D plot of maximum error (a) and absolute error (b) of Example 5.1

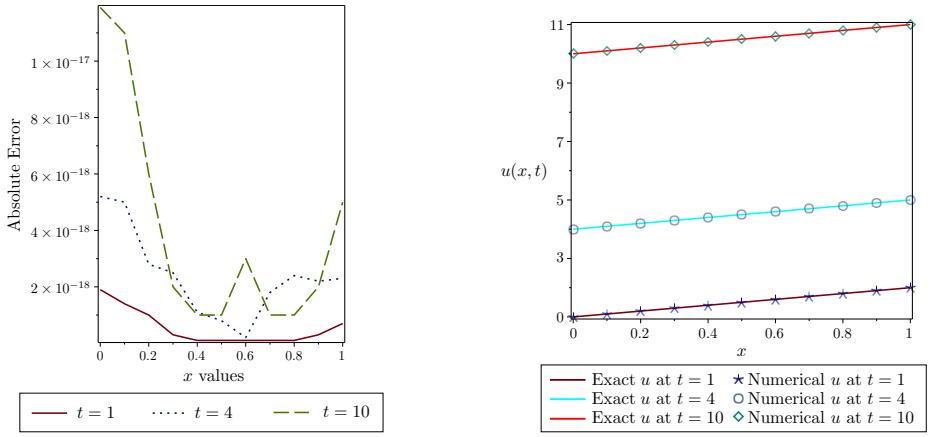

(a) (b)

FIGURE 2. Absolute error (a) and exact and numerical solutions (b) at t=1,4,10 with $\Delta t = 0.1$ and $n = 10$ of Example 5.1

Example 5.2. *Consider the backward Kolmogorov* (4) *as follows:*

$$\frac{\partial}{\partial t}u(x,t) = -\Big[A(x,t)\frac{\partial}{\partial x} + B(x,t)\frac{\partial^2}{\partial x^2}\Big]u(x,t),$$

with $A(x,t) = -(x+1)$, $B(x,t) = x^2e^t$ *and* $u(x,0) = x+1$, *which has the exact solution* $u(x,t) = (x+1)e^t$. *The* L_∞ *and* L_2 *errors are listed in Table 3, at different times, and compared with the results in* [2]. *It is observable that the present method is more accurate in comparison with* [2]. *In* [2], $\Delta t = 0.01$ *was used, whereas in MQQI method* $\Delta t = 0.1$ *is used. Table 4 presents spatial rate of convergence obtained using our scheme with* $\Delta t = 0.1$ *and different values of* n *for* $t = 0.3$. *It can be concluded from Table 4 that the convergence rate decreases with the smaller spatial step size. The graphs of top view of maximum error and absolute error over the space time with a color bar are shown in Figure 3. We also plot the graphs of absolute error and the estimated and analytical function at* $t = 1, 4, 10$ *in Figure 4.*

TABLE 3. The comparisons of the L_∞, L_2 errors of the presented method with the results of [2] at different times of Example 5.2.

t	*MQQI*		*method of* [2]	
	L_∞	L_2	L_∞	L_2
1	*2.292e-16*	*1.610e-16*	*4.421e-10*	*2.825e-10*
2	*2.903e-16*	*1.973e-16*	*5.511e-10*	*3.109e-10*
3	*3.410e-16*	*2.497e-16*	*4.032e-9*	*2.830e-9*
5	*4.900e-16*	*3.241e-16*	*4.984e-8*	*2.912e-8*
7	*4.500e-15*	*2.967e-15*	*4.019e-7*	*2.829e-7*
10	*8.100e-14*	*5.799e-14*	*4.967e-6*	*2.913e-6*

TABLE 4. The spatial rate of convergence at $t = 0.3$ with $\Delta t = 0.1$ of Example 5.2.

n	L_∞	*Order*	L_2	*Order*
10	*6.48e-11*	—	*4.68e-11*	—
20	*1.66e-10*	*1.36*	*1.19e-10*	*1.35*
30	*2.82e-10*	*1.30*	*2.02e-10*	*1.30*
40	*4.08e-10*	*1.28*	*2.92e-10*	*1.27*
50	*5.42e-10*	*1.26*	*3.87e-10*	*1.25*

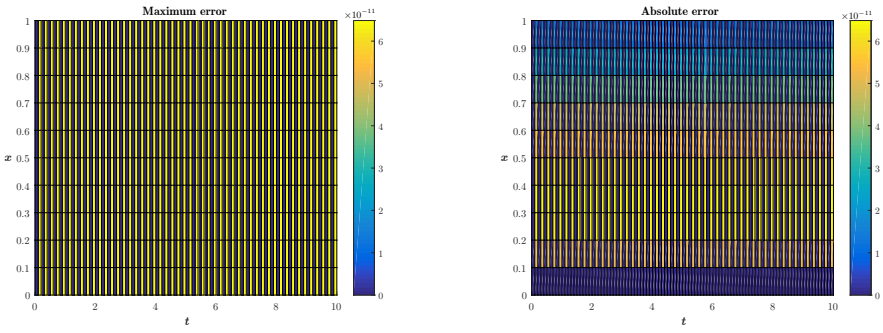

(a) (b)

FIGURE 3. Top view of the 3D plot of maximum error (a) and absolute error (b) of Example 5.2

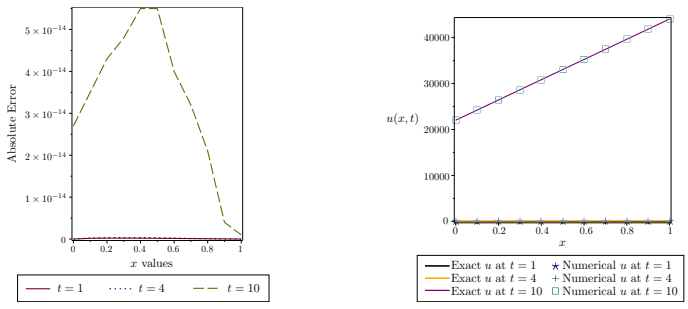

(a) (b)

FIGURE 4. Absolute error (a) and exact and numerical solutions (b) at t=1,4,10 with $\Delta t = 0.1$ and $n = 10$ of Example 5.2

Example 5.3. *Consider the Eq.* (7) *with* $A = \frac{7}{2}u$, $B = xu$ *and* $u(x,0) = x$, *which has the exact solution* $u(x,t) = \frac{x}{t+1}$. *The* L_∞ *and* L_2 *errors are listed in Table 5, at different*

times, and compared with the results in [2]. *The graph of maximum error is ploted in Figure 5 and The graphs of top view of maximum error and absolute error are shown in Figure 6. In* [2], *time step* $\Delta t = 0.01$ *was used, whereas in MQQI method* $\Delta t = 0.1$ *is used.*

TABLE 5. The comparisons of the L_∞, L_2 errors of the presented method with the results of [2] at different times of Example 5.3.

t	*MQQI*		*method of* [2]	
	L_∞	L_2	L_∞	L_2
1	*2.521e-10*	*1.856e-10*	*4.500e-13*	*2.669e-13*
2	*2.990e-10*	*2.201e-10*	*6.007e-11*	*2.852e-11*
3	*3.154e-10*	*2.322e-10*	*2.250e-13*	*1.335e-13*
5	*3.271e-10*	*2.408e-10*	*5.997e-11*	*2.384e-11*
7	*3.312e-10*	*2.438e-10*	*1.125e-13*	*6.674e-14*
10	*3.336e-10*	*2.456e-10*	*4.955e-12*	*2.881e-12*

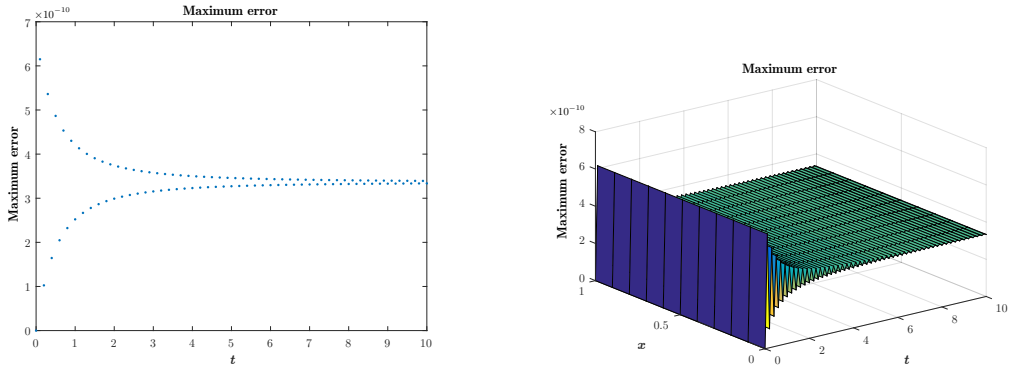

(a) (b)

FIGURE 5. Maximum error of Example 5.3

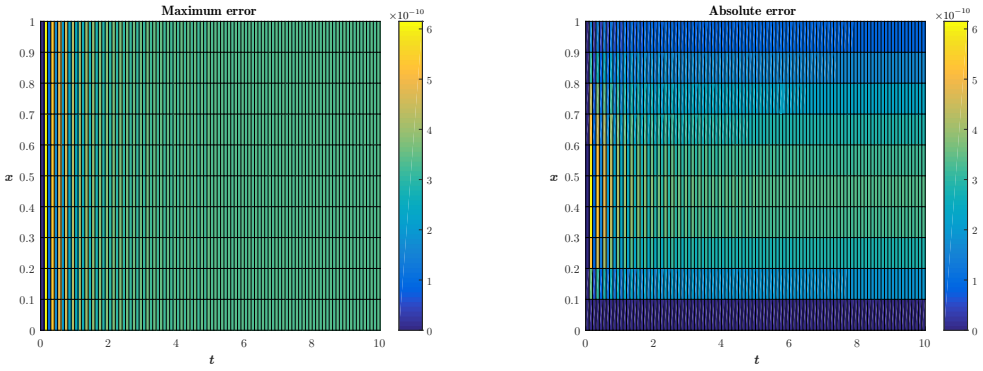

(a) (b)

FIGURE 6. Top view of the 3D plot of maximum error (a) and absolute error (b) of Example 5.3

6. Conclusion

We have presented a numerical scheme based on high accuracy multiquadric quasi-interpolation scheme for solving the FPE. θ-weighted finite difference scheme is employed for discretization the temporal derivative and then the solution of the Eq. (3) is approximated using multiquadric quasi-interpolation operator $\mathcal{L}_{W_2}$.
During the calculation, it is obvious that our scheme is simple and easy to implement. The efficiency and accuracy of the proposed method have been demonstrated through the three examples. Also, the tables show that this scheme performs better than the method of [2]. Moreover, we have used a bigger time step Δt, in comparison with the method of [2]. The univariate multiquadric quasi-interpolation scheme is only used to solve one dimensional FPEs. In future, we will focus on the higher dimensions of FPEs.

References

[1] Aminataei, A. and Mazarei, M. M., (2005), Numerical solution of elliptic partial differential equations using direct and indirect radial basis function networks, Eur. J. Sci. Res., 2, pp. 5-15.
[2] Askari, M. and Adibi, H., (2015), Meshless method for the numerical solution of the Fokker-Planck equation, Ain Shams Eng. J., 6, pp. 1211-1216.
[3] Ballestra, L. V. and Pacelli, G., (2012), A radial basis function approach to compute the first-passage probability density function in two-dimensional jump-diffusion models for financial and other applications, Eng Anal Bound Elem, 36, pp. 1546-1554.
[4] Beatson, R. and Powell, M., (1992), Univariate multiquadric approximation: Quasi-interpolation to scattered data, Constr Approx, 8, pp. 275-288.
[5] Biazar, J., Gholamin, P. and Hosseini, K., (2010), Variational iteration method for solving Fokker-Planck equation, J Franklin Inst, 347, pp. 1137-1147.
[6] Buhmann, M. D., (2003), Radial Basis Functions: Theory and Implementations, Cambridge University Press, Cambridge, United Kingdom.
[7] Dehghan, M. and Tatari, M., (2006), The use of He's variational iteration method for solving a Fokker-Planck equation, Phys Scr, 74, pp. 310-316.
[8] Fasshauer, G. E., (2007), Meshfree Approximation Methods with MATLAB, World Scientific Publishing, Singapore.
[9] Gardiner, C. W., (2004), Handbook of stochastic methods for physics, chemistry and the natural sciences, Vol.13 of Springer Series in Synergetics. Springer-Verlag, third edition.
[10] Hardy, R. L., (1971), Multiquadric equations of topography and other irregular surfaces, J. Geophys. Res., 76, pp. 1905-1915.
[11] Harrison, G. W., (1988), Numerical solution of the Fokker Planck equation using moving finite elements, Numer Methods Partial Differ Equ, 4, pp. 219-232.
[12] Hon, Y. C. and Mao, X. Z., (1998), An efficient numerical scheme for Burgers' equation, Appl. Math. Comput., 95, pp. 37-50.
[13] Jafari, M. A. and Aminataei, A., (2009), Application of homotopy perturbation method in the solution of Fokker-Planck equation, Phys. Scr., 80, 055001 (5pp).
[14] Jiang, Z. W., Wang, R. H., Zhu, C. G. and Xu, M., (2011), High accuracy multiquadric quasi-interpolation, Appl. Math. Model., 35, pp. 2185-2195.
[15] Jumarie, G., (2004), Fractional Brownian motions via random walk in the complex plane and via fractional derivative. Comparison and further results on their Fokker-Planck equations, Chaos Solitons Fractals, 22, pp. 907-925.
[16] Kamitani, Y. and Matsuba, I., (2004), Self-similar characteristics of neural networks based on Fokker-Planck equation, Chaos Solitons Fractals, 20, pp. 329-335.
[17] Madych, W. R. and Nelson, S. A., (1990), Multivariate interpolation and conditionally positive definite functions. II, Math Comput, 54, pp. 211-230.
[18] Palleschi, V., Sarri, F., Marcozzi, G. and Torquati, M.R., (1990), Numerical solution of the Fokker-Planck equation: A fast and accurate algorithm, Phys. Lett., 146, pp. 378-386.
[19] Rahimi, M. and Adibi, H., (2020), Solving one dimensional nonlinear coupled Burgers equations using high accuracy multiquadric quasi-interpolation, Comput. Methods Differ. Equ, 8, pp. 347-363.

[20] Rashidinia, J., Ghasemia, M. and Jalilian, R., (2010), Numerical solution of the nonlinear Klein-Gordon equation, J. Comput. Appl. Math., 233, pp. 1866-1878.
[21] Reif, J. and Barakat, R., (1977), Numerical solution of the Fokker-Planck equation via Chebyschev polynomial approximations with reference to first passage time probability density functions, J. Comput. Phys., 23, pp. 425-445.
[22] Risken, H., (1989), The Fokker-Planck equation: methods of solution and applications, Heidelberg: Springer Verlag, Berlin.
[23] Sarboland, M. and Aminataei, A., (2014), On the numerical solution of one-dimensional nonlinear nonhomogeneous Burgers' equation, J Appl Math, 2014, Article ID 598432, 15 pages.
[24] Tatari, M., Dehghan, M. and Razzaghi, M., (2007), Application of the Adomian decomposition method for the Fokker-Planck equation, Math Comput Model, 45, pp. 639-650.
[25] Twizell, E. H., (1984), Computational methods for partial differential equations, Ellis Horwood Limited, England.
[26] ul-Islam, S., Haq, S. and Uddin, M., (2009), A meshfree interpolation method for the numerical solution of the coupled nonlinear partial differential equations, Engineering Analysis with Boundary Elements, 33, pp. 399–409.
[27] Vanani, S. K. and Aminataei, A., (2010), On the numerical solution of delay differential equations using multiquadric approximation scheme, Functional Differential Equations, 17, pp. 391-399.
[28] Wendland, H., (2005), Scattered Data Approximation, Cambridge Monographs on Applied and Computational Mathematics, Cambridge University Press, Cambridge, United Kingdom.
[29] Wu, Z., (1995), Compactly supported positive definite radial functions, Advances in Computational Mathematics, 4, pp. 283-292.
[30] Wu, Z. and Schaback, R., (1994), Shape preserving properties and convergence of univariate multiquadric quasi-interpolation, Acta Mathematicae Applicatae Sinica, 10, pp. 441-446.
[31] Xiao, M. L., Wang, R. H. and Zhu, C. G., (2011), Applying Multiquadric Quasi-Interpolation to Solve KdV Equation, Journal of Mathematical Research & Exposition, 31, pp. 191-201.
[32] Xu, Y., Ren, F. Y., Liang, J.R. and Qiu, W.Y., (2004), Stretched Gaussian asymptotic behavior for fractional Fokker-Planck equation on fractal structure in external force fields, Chaos, Solitons and Fractals, 20, pp. 581-586.
[33] Zorzano, M. P., Mais, H. and Vazquez, L., (1999), Numerical solution of two dimensional Fokker-Planck equations, Applied Mathematics and Computation, 98, pp. 109-117.

Mahbubeh Rahimi received her B.Sc. degree in mathematics from Kashan University, Iran in 2010. She received her M.Sc. degree from Isfahan University in 2012. Currently she is a Ph.D. student in applied mathematics in the department of mathematics, Islamic Azad university, Central Tehran Branch, Iran. Her fields of interest are numerical methods for the solution of ordinary and partial differential equations.

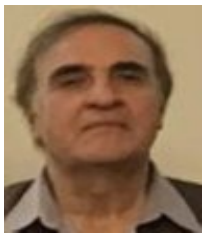

Hojatollah Adibi was born in 1948 and obtained his B.Sc. & M.Sc. in 1970 &1974 respectively in Iran. Prof. Adibi was employed by the Amirkabir University of Technology in 1976 and obtained his Ph.D. from the City University, England in Applied Mathematics.

Majid Amirfakhrian received his MSc in Applied Mathematics from the Sharif University of Technology and completed his Ph.D. at Azad University in Science and Research branch. Later, he joined Azad University, Central Tehran Branch (IAUCTB) in 2002 and he became a full professor in 2015. He is currently a Visiting Researcher at the University of Calgary, Canada. Some of his specific interests are solving the problems of Fuzzy Approximation, Data Sciences, Multivariate Approximation, Image Processing and Numerical Partial Differential Equations.